Valence-band electronic structure of Co_3O_4 epitaxy on CoO(100)

M. A. Langell,* M. D. Anderson, G. A. Carson, L. Peng, and S. Smith
Department of Chemistry and Center for Materials Research and Analysis, University of Nebraska, Lincoln, Nebraska 68588-0304
(Received 16 June 1998)

Valence-band photoemission studies have been performed on a CoO(100) single crystal as it is slowly oxidized under 1×10^{-4} Torr O_2 at 623 K, eventually forming a Co_3O_4 epitaxial film. The most significant changes occur in $3d$-related features, with the peak located at the top of the valence band sharpening and shifting to lower binding energies as the spinel oxide forms. Constant initial-state measurements indicate that Co_3O_4 contains admixture from neighboring O $2p$ in its $3d$ band, as observed for CoO and other monoxide charge-transfer insulators. Unlike the rocksalt monoxides, which have only a single type of cobalt (Co^{2+}) located in octahedral lattice sites, the spinel Co_3O_4 has both octahedral Co^{3+} and tetrahedral Co^{2+} sublattices. The peak at the top of the Co_3O_4 valence band results from the $3d^6\underline{L}$ final state of the octahedral Co^{3+} $3d$ band. Although some states derived from tetrahedral Co^{2+} may be present at the top of the valence band, the greatest contribution from the tetrahedral Co^{2+} sublattice appears at approximately -3.8 eV, overlapping with O $2p$ derived features of the spectrum. The Co^{3+} $3d^{n-1}$ satellite is much less intense in Co_3O_4 than in CoO, as is observed for the analogous structure in the cobalt $2p$ core spectra. An oxygen $2p$-derived structure remains fairly constant throughout the oxidation process, with the exception of an intermediate species, which imparts a broad, humplike appearance centered at -5.3 eV to the O $2p$ region and disappears as oxidation to Co_3O_4 is completed. The origin of the feature is not clear; however it is most likely due either to an adsorbate or to a defectlike intermediate in the oxidation process. [S0163-1829(99)06703-X]

I. INTRODUCTION

The valence-band electronic structure of the cubic $3d$ transition-metal monoxides MnO, FeO, CoO, and NiO has been intensively studied by both experimental and theoretical methods.[1–21] These materials, although not well served by standard one-electron band theory, can successfully be described by the charge-transfer insulator model in which strong electron correlation localizes the $3d$ electrons within the partially filled valence band. Some admixture from neighboring oxygen $2p$ orbitals provides the ''charge-transfer'' descriptive and results in a hybridized view of the transition-metal-derived valence band:

$$\varphi=\alpha 3d^n+\beta 3d^{n+1}\underline{L}+\gamma 3d^{n+2}\underline{L}^2\ldots, \qquad (1)$$

where $\alpha,\beta,\gamma,\ldots$, are coefficients representing the admixture of a particular configuration to the ground-state wave function, ψ, n is the number of $3d$ electrons associated with the metal cation in the monoxide, and $\underline{L}$ represents a hole on a neighboring oxygen anion due to electron donation into the $3d$ band. This leads to a large valence bandwidth and interesting valence and core level satellite features in photoemission spectra. Cobalt monoxide, in which the cation is formally in the 2^+ oxidation state, is nominally $3d^7$ in the ground-state wave function for the α term.

With the exception of NiO, the rocksalt monoxides are not the only binary oxide phases that form under readily attainable oxygen partial pressures. Under common ambient conditions, the thermodynamically favored form of the oxide is often the spinel, M_2O_4 (M=Mn, Fe, Co). Even when mass transport limits the bulk of the oxide to a metastable monoxide form, the surface can and often does contain significant amounts of the spinel phase.[22–24] Unfortunately, few studies have been aimed at elucidating the valence band structure of spinels.[19,21,24,25] Despite their simple apparent stoichiometry, the spinels are considerably more complicated to model than are the monoxides. Spinel oxides have all the disadvantages of the rocksalt monoxides with their partially filled $3d$ states and significant electron correlation effects. Additionally, the spinels feature two metal oxidation states (M^{2+}/M^{3+}) and two different cation sites (tetrahedral/octahedral) each type of which is only partially occupied to give a unit cell of 56 atoms.

We present here valence-band photoemission studies of CoO(100) as it is oxidized to form a thin film epitaxy of Co_3O_4(100). The x-ray photoelectron spectra (XPS) of the Co $2p$ and O $1s$ core levels, low-energy electron diffraction (LEED) and high-resolution electron-energy-loss spectra (HREELS) of similarly prepared epitaxies have been previously presented,[22] and the resultant films has been shown to be stoichiometric, well ordered, and generally characteristic of a Co_3O_4 spinel sample. Both rocksalt CoO and spinel Co_3O_4 have a comparable oxygen sublattice with fcc closest packed structure in which O^{2-}-O^{2-} nearest neighbor distances match to within 5%.[26] In the monoxide, Co^{2+} cations occupy all octahedral sites, whereas in the Co_3O_4 spinel half the octahedral sites are populated with Co^{3+} and one eighth the tetrahedral sites are populated with Co^{2+} in a specific, well-ordered manner. Under oxidizing conditions that also allow for sufficient mobility of the cobalt cations in the near-surface region, it is possible to evolve from CoO(100) to Co_3O_4(100) smoothly and with little loss of structural integrity through slow surface oxidation. The evolution of the valence-band photoemission for this process is reported below.

II. EXPERIMENT

CoO single crystals were obtained from Atomergic Chemetals Corporation and were oriented to within 1° of the (100) plane by Laue back diffraction. The surface was polished with successively finer grades of alumina to 0.03-μm alumina particle size and placed in a UHV chamber for further substrate pretreatment. *In situ*, the CoO(100) sample was cleaned by repeated cycles of Ar^+ bombardment (5×10^{-5} Torr, 1 keV, 8 μamp, 15 min), O_2 anneal (5×10^{-7} Torr, 523 K, 15 min), and UHV anneal ($\leqslant 3\times10^{-10}$ Torr 523 K, 15 min) until no impurities were detected by Auger electron spectroscopy and an appropriate (1×1) LEED pattern was observed. Prior to the initial photoemission measurements and subsequent surface oxidation, a final 10-min anneal at 850 K was conducted. This pretreatment protocol has previously been shown[22,24] to yield stoichiometric and well-ordered CoO(100) of sufficient integrity to serve as a substrate for the Co_3O_4 thin film formation described below.

Ultraviolet photoemission spectra (UPS) were acquired at the National Synchrotron Light Source (NSLS) of Brookhaven National Laboratory on beamline *U7b* with initial photon energies of 30–100 eV using a three-plane grating monochromator with the slit set to 220 μm. This yields an incident beam resolution of approximately 178 meV at 30-eV primary beam energy. The UPS was taken with an incident beam angle of 56° relative to the surface normal and with photoemission detected in the normal emission mode. For substrates with fourfold symmetry like CoO(100), this mixes allowed (detectable) initial states of $\Delta5$ and $\Delta1$ symmetry, with a slight weighting towards states with $\Delta1$ symmetry.[27] The Vacuum Generators APES 400 hemispherical analyzer was run at a pass energy of 12 eV, giving a spectral resolution of 0.12 eV. UP spectra were acquired as an average of 4–8 scans with approximately 300 points taken across the spectrum. UP spectral intensities have been corrected for variation in photon flux with synchrotron beam current. All photoemission data were taken at room temperature.

CoO(100) surface oxidation was performed at 1×10^{-4} Torr O_2 at 623 K for periods of up to 4 h. The crystal was heated conductively by an assembly held in close contact with the back of the 0.1-cm-thick crystal. Temperatures were measured with a chromel-alumel thermocouple pressed against the crystal back. During oxidation, the sample was translated under UHV into the top part of the two-story bell jar, which could be isolated by a poppet valve from the lower story containing the electron spectrometers and LEED optics. Base pressure in the upper story was $\leqslant1\times10^{-9}$ Torr when valved off from the lower part of the bell jar; the entire bell jar base pressure was $\leqslant2\times10^{-10}$ Torr in UHV heating experiments on the $CoO/Co_3O_4(100)$ epitaxial films and during the acquisition of photoemission data.

III. CoO(100) SURFACE OXIDATION TO THE Co_3O_4 SPINEL STRUCTURE

We focus this study on changes that occur in valence-band photoemission as CoO(100) is oxidized, with an emphasis on the characterization of the valence-band structure of Co_3O_4 epitaxial films that result upon saturation oxidation. Co_3O_4 is difficult to obtain in single-crystal form and thus studies of well-ordered Co_3O_4 surfaces are rare. In these experiments, UP spectra from surface-oxidized CoO and from CoO/Co_3O_4 epitaxies were easier to obtain in high quality than were those from the initial CoO(100) surface due to the greater conductivity of the oxidized layers. While binding-energy shifts were compensated by referencing to the valence-band maximum, CoO(100) spectra were typically lower in the signal-to-noise ratio and often were not obtainable for high primary photon-beam energies. The CoO(100) valence band UP spectrum has been previously elucidated and more detailed studies of the stoichiometric CoO(100) surface band structure can be found elsewhere.[1–3] Figure 1 shows a typical spectrum for the substrate used in the present oxidation studies, with relevant features of the CoO valence-band structure indicated in the figure. These and all subsequent photoemission data are reported relative to the valence-band maximum, V_m, as is common practice with the poorly conducting oxide substrates.

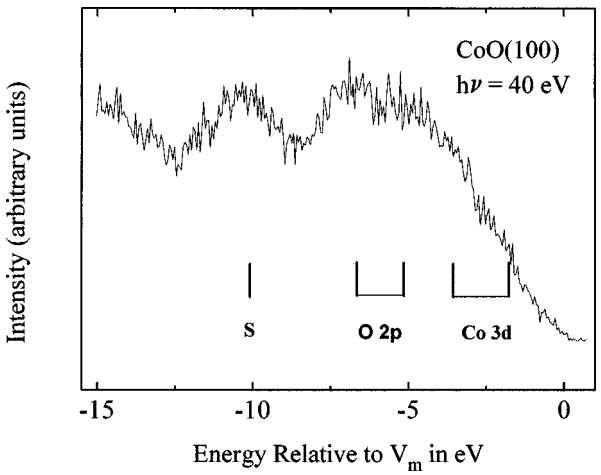

FIG. 1. Normal emission valence-band spectrum of the CoO(100) substrate taken at a primary beam energy of 40 eV.

The top of the CoO valence band is comprised primarily of states derived from cobalt $3d\ t_{2g}$ minority spin. However, the charge-transfer nature of CoO causes features resulting from both $3d^6$ and $3d^7\underline{L}$ final states to be observed in photoemission from this band. Photoemission from the top of the valence band results from the $3d^7\underline{L}$ final state[1,4] and its peak maximum is observed here at -1.7 eV. The broad character of this feature is typical of that observed in normal emission from CoO(100),[28] particularly for spectra generated at photon energies below the cobalt $3p$ resonance at approximately 60 eV. The $3d^6$ final-state feature is observed at -10.4 eV and is labeled as a satellite (*S*) in Fig. 1 in analogy with structure that appears to higher binding energies in core-level photoemission data. An additional $3d$-derived feature is found at -3.8 eV, resulting from cobalt $3d$ orbitals with e_g character.[5] Oxygen $2p$-derived bands are observed at -5.1 and -7.6 eV for the 40-eV-initiated spectrum. The energies of these features are in good agreement with previously reported values.[2]

Figure 2 shows photoemission from the CoO(100) substrate annealed at 623 K under 1×10^{-4} Torr O_2 for periods of up to 4 h, after which no additional changes in the spec-

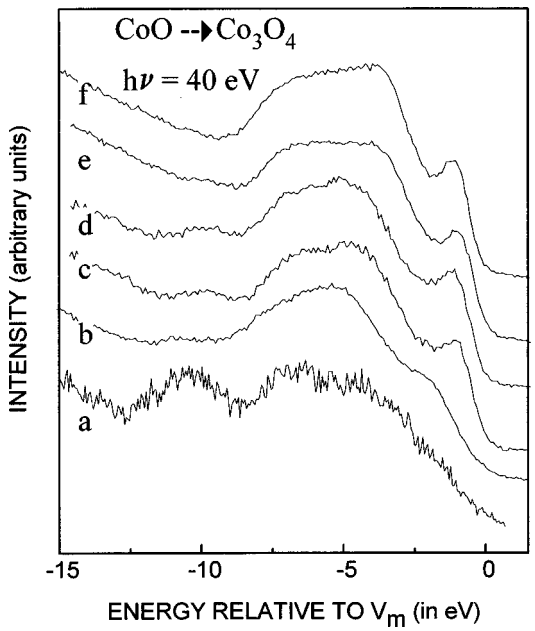

FIG. 2. Valence-band spectra at 40 eV for the CoO(100) substrate heated at 623 K and 1×10^{-4} Torr O_2 for (a) 0 h, (b) 0.5 h, (c) 1.0 h, (d) 2.0 h, (e) 3.0 h, and (f) 4.0 h. The latter spectrum corresponds to epitaxial Co_3O_4.

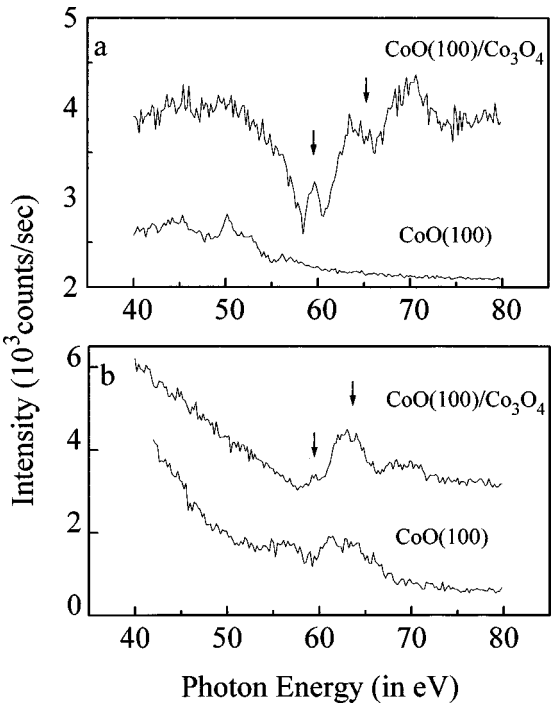

FIG. 3. Constant state initial spectroscopy (CIS) measurements at (a) -1.0 eV and (b) -9.6 eV. The arrows point to the approximate locations of the antiresonance or resonance structure.

trum could be detected. During this oxidation procedure, a visual inspection of the LEED pattern indicated the surface remained ordered with (100) symmetry throughout the oxidation process, although less than optimum conditions for acquiring LEED on the synchrotron floor prevented a detailed analysis of the LEED superstructure resulting from spinel formation. XPS/HREELS studies of CoO(100) under similar oxidation conditions have indicated the epitaxy resembles Co_3O_4 in its phonon spectrum and in characteristic XPS satellite structure, core level binding energies and O/Co core photoemission intensities.[22]

The most dramatic change in the photoemission spectrum is the development of a new, sharp valence-band peak at -1.0 eV, which increases in intensity with oxidation at the expense of the -1.7-eV $3d^7\underline{L}$ peak of the CoO substrate. Both Co_3O_4 and CoO $3d^7\underline{L}$ features can be observed in the spectrum at intermediate oxidation times, most obvious perhaps in Fig. 2(c) and neither feature is observed to shift during the oxidation process. The -1.7-eV feature is, therefore, believed to be characteristic of the CoO(100) substrate and the -1.0-eV feature is intrinsic to the thin, oxidized Co_3O_4 film that forms epitaxially on top of it.

The -1.0-eV peak from the Co_3O_4 epitaxy shows classic constant initial state (CIS) spectroscopic behavior (Fig. 3) that is characteristic of strongly electron-correlated charge-transfer oxides.[1,2,4,18–20,29] The resonant behavior results from the opening of a second pathway to the $3d^{n-1}$ final state above the cobalt $3p$ threshold:

$$3p^6 3d^n + h\nu \rightarrow 3p^5 3d^{n+1} \rightarrow 3p^6 3d^{n-1} + e^- \qquad (2)$$

in addition to the direct pathway available both above and below this threshold:

$$3p^6 3d^n + h\nu \rightarrow 3p^6 3d^{n-1} + e^- . \qquad (3)$$

Since both pathways lead to indistinguishable final states, quantum interference between the two channels can result in either enhancement or suppression of the $3d$ valence-band transitions at the $3p$ threshold. Metal photoemission features with $3d^n\underline{L}$ final-state character tend to exhibit suppression, whereas those with $3d^{n-1}$ final-state character tend to undergo resonant enhancement.[30] The main peak at -1.0 eV undergoes an antiresonance at the cobalt $3p$ threshold and is, therefore, assigned to $3d$-derived band structure associated with the $3d^n\underline{L}$ final state.

The satellite $3d^6$ final-state feature associated with the CoO(100) photoemission spectrum also undergoes a dramatic change as the substrate is oxidized. Initially at -10.4 eV and quite intense, the satellite shifts to lower energies and decreases in intensity with increased surface oxidation. Throughout the oxidation process the satellite retains its $3d$ character, as is demonstrated by its resonance-enhanced behavior in CIS (Fig. 3). Because the satellite is no longer detectable in the fully oxidized Co_3O_4 epitaxy, the CIS data of Fig. 3b have been acquired after 3 h of oxidation, at which point the satellite has shifted to -9.6 eV. The resonance shows a doublet structure, with a small but distinct peak at 59.5 eV and a larger resonance at 63 eV. While the small 59.5-eV peak is comparable to the background noise level in the present CIS spectrum, it is obtained reproducibly. The doublet structure of the resonance is more clearly observed in CoO(100) CIS data,[1] and while the origins of the doublet remain unknown it has been postulated to result from the two spin-orbital components of the Co $3p$ initial state. Note that in Fig. 3(b) the CIS data for the CoO(100) substrate are taken at -9.6 eV for comparison to the CoO(100)/Co_3O_4

data and do not represent CIS from the CoO(100) satellite at −10.4 eV, which shows the much stronger resonance behavior previously reported.[1] The small increase in intensity in the CIS for the CoO(100) substrate at −9.6 eV is most likely due to residual intensity from the −10.4-eV satellite peak.

Other changes in the valence-band photoemission that occur with surface oxidation of the CoO(100) substrate are an increased intensity in the region of the −3.8 eV $3d$ peak and the appearance of an intermediate state in the O $2p$ region that gives the central portion of the UP spectrum a single-peaked, rounded characteristic with a maximum in intensity at approximately −5.3 eV. This is most evident during initial oxidation stages [e.g., 0.5 h; Fig. 2(b)] and is similar in appearance to changes previously reported for UPS data taken following O_2 chemisorption on defect CoO(100) at 300 K.[2] The intermediate state is clearly associated with a chemisorbed form of oxygen or a lattice oxide defect in route to spinel formation since it appears in the early stages of oxygen exposure but disappears as the substrate reaches saturation oxidation concentrations. At oxidation saturation, the O $2p$ region is comparable to that of the initial CoO(100) substrate.

Neither oxygen-derived nor the −3.8-eV $3d$-derived states show resonant photoemission behavior at the cobalt $3p$ threshold. This is expected for states arising from oxygen-derived orbitals, but not necessarily from those with cobalt $3d$ character. However, similar CIS spectra have been obtained for cobalt monoxide[1,2] and nickel oxide[4,25] for transitions in this part of the valence-band structure. The lack of resonant behavior at the $3p$ threshold for the metal-derived states was attributed to the difficulty in separating potential resonant effects in the $3d$ band from that of the nonresonant but overlapping oxygen $2p$ states.

IV. CHARACTERIZATION OF THE Co_3O_4 SPINEL PHOTOEMISSION

Saturation oxidation of the CoO(100) substrate is accompanied by several changes attributable to Co_3O_4 formation. The O $1s$/Co $2p$ XPS and Auger O KL_2L_2/Co $L_3M_{4,5}M_{4,5}$ intensity ratios increase by approximately 4/3 rds to reflect the change from monoxide to spinel stoichiometry. Qualitative changes in the Co $2p$ core-level peak shape are also characteristic of a CoO→Co_3O_4 transformation,[22,23,27,30–33] as shown by XPS for the initial and oxygen-saturated CoO(100) surfaces in Fig. 4. The satellite structure in these data arises from final-state effects analogous to those discussed above for the valence band, and the satellites labeled S in Figs. 1 and 4 have common origins. CoO and Co_3O_4 have different coupling into the two possible final states giving rise to the main and satellite peaks, with the Co_3O_4 spinel structure more greatly favoring the lower binding energy $2p^5 3d^{n+1}\underline{L}$ final state and thus having considerably lower intensity in the higher binding energy $2p^5 3d^n$ satellite when compared to the CoO rocksalt substrate. In addition to a decreased satellite intensity observed for Co_3O_4, a shoulder which has previously been assigned to tetrahedral Co^{2+}-related states[32,33] appears to lower binding energy. This peak, which is more clearly resolved in the $2p_{3/2}$ region due to lack of overlap with other spectral features, is observed with a binding energy of 779.6 eV. Photoemission

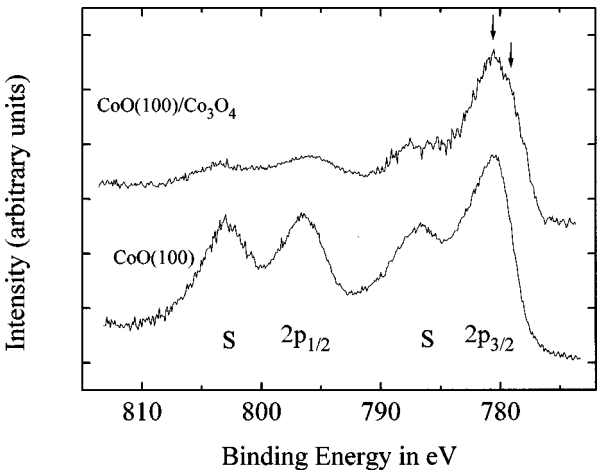

FIG. 4. XP core region for CoO(100) and the Co_3O_4 epitaxy taken with Mg K_α radiation and a band pass of 50 eV. The arrows in the spectrum for CoO(100)/Co_3O_4 epitaxy indicate core emission associated primarily with Co^{3+} (779.6 eV) and Co^{2+} (780.5 eV) cations in the spinel structure.

from the octahedrally coordinated cobalt species, Co^{2+} in CoO and Co^{3+} in Co_3O_4, yields $2p_{3/2}$ and $2p_{1/2}$ binding energies of 780.5 eV and 796.5 eV for the monoxide and of 780.5 eV and 795.7 eV for the Co_3O_4 spinel, in good agreement with previously reported literature values for these materials.[27]

Valence-band spectra for the CoO(100) substrate and the fully oxidized CoO(100)/Co_3O_4 epitaxial layer are compared in Fig. 5 to illustrate differences in spectral features between the two materials. The top of the valence band sharpens considerably and shifts to −1.0 eV upon Co_3O_4 formation. While the complexity of the spinel makes theoretical analysis of the valence-band structure difficult, a simple estimation of $3d$ basis states is possible by considering the local

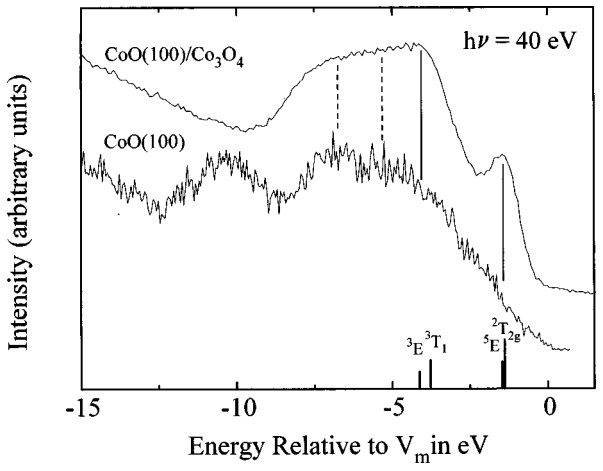

FIG. 5. Comparison of 40 eV-initiated photoemission from the valence band of CoO(100) and the Co_3O_4 epitaxy. Solid lines connecting the two spectra indicate the position of $3d$-derived features. Dotted lines indicate the approximate position of the O $2p$-derived states. Along the bottom of the figure, final states for the spinel Co^{3+} ($^2T_{2g}$) and the Co^{2+} (^5E, $^3T_1$, ^3E) sub-bands are made with ligand field theory, after Ref. 21.

environment of the tetrahedral Co^{2+} and octahedral Co^{3+} with ligand field theory. Using Tanabe-Sugano diagrams and appropriate Racah parameters,[34] final-state configurations predicted to be observable in Co_3O_4 valence-band photoemission spectra[21] are shown along the bottom of Fig. 5. Note that structure at the top of the valence band is comprised primarily of features derived from $3d$ levels of the Co^{3+} octahedral cation, specifically with the $^2T_{2g}$ configuration of the $(t_{2g})^5$ final state. Analogous valence-band photoemission studies of Fe_3O_4 (Ref. 2) and of $LiCoO_2$ (Ref. 20) support assigning this peak to $3d$-derived states from Co^{3+}. However, overlap with photoemission from tetrahedral Co^{2+} resulting in an $(e)^3(t_2)^3$ final state with ^5E configuration may result in some contribution from both octahedral Co^{3+} and tetrahedral Co^{2+} derived states at the valence band maximum. The tetrahedral $Co^{2+}(e)^3(t_2)^3$ final state with ^3E configuration and the $(e)^4(t_2)^2$ final state with $^3T_1$ configuration are predicted to occur 2–3 eV below the ^5E final state transition.[21]

The antiresonance behavior observed for the -1.0 eV peak in CIS (Fig. 3) indicates that $3d$-derived states at the top of the valence-band show admixture with lattice oxygen $2p$ orbitals. Conceivably both octahedral $Co^{3+}(3d^6)$ and $Co^{2+}(3d^7)$ could contribute to the basis set for the initial state(s) of this resonance. However, similarity to valence-band photoemission peak shape and antiresonance behavior observed in photoemission studies of $LiCoO_2$, which contain only Co^{3+} in near-octahedral environments, indicates the effect is dominated by cobalt in the octahedral sites which overlap more effectively with O $2p$ orbitals. For simplicity, the final state of the main peak will therefore be labeled $3d^5\underline{L}$, although any contributions from the Co^{2+} tetrahedral sublattice should more properly be indicated as $3d^6\underline{L}$. Regardless of how the intensity of the -1.0 eV peak is partitioned, the antiresonance behavior of the peak gives evidence that the Co_3O_4 spinel is analogous in its bonding to the related rocksalt monoxide compounds, which are charge-transfer insulators.

The location of the $3d^5$ final-state satellite for the Co_3O_4 surface is not obvious. It could continue to shift to lower binding energy with increased oxidation to overlap at saturation with the more intense O $2p$ states. It could be present below the noise level of the spectrum or lost in the sloping background of secondary electrons. A final possibility is that it might be barely detectable as a very broad resonance centered around approximately 12 eV most noticeable at higher primary beam energies evident in Fig. 6. The slope of the background emission decreases as the primary beam energy increases and resonance effects also predict higher intensity for $3d$-derived satellites at or above approximately 60 eV. This may make detection of the satellite a delicate balance of factors. There is a very weak, broad structure visible in the 80 eV spectrum of Fig. 6 that could potentially be the $3d^5$ satellite. However, changes in background emission, along with the weak intensity of the photoemission feature lead to inconclusive CIS analysis. Either coupling to this final state is too weak in the spinel structure for it to be observed with certainty or it overlaps with and thus is obscured by other features of the spectrum.

Photoemission data for the $CoO(100)/Co_3O_4$ surface were taken for spectra initiated with photons in the range of 30–100 eV (Fig. 6). The antiresonance due to $3p$ excitation at approximately 60 eV is clearly evident for the $3d^n\underline{L}$ state at the top of the valence band. In addition, the oxygen $2p$ region appears to be undergoing some change in peak shape as the photon excitation energy is varied. Both experimental[1] and theoretical[1,3] band-structure studies of CoO have determined that oxygen-derived states show measurable dispersion whereas states that are primarily $3d$ in character are relatively nondispersive. Unfortunately, no band structure calculations have appeared for Co_3O_4 or any other spinel oxides. To a first approximation, the O $2p$-derived bands of the spinel and of the monoxide can be assumed to be comparable since both structures are cubic close packed in lattice O^{2-}. Indeed for spectra initiated with comparable photon energies, normal emission data for CoO(100) and the presently reported $CoO(100)/Co_3O_4$ valence-band spectra are very similar in the oxygen $2p$ range (Fig. 5, dashed lines).

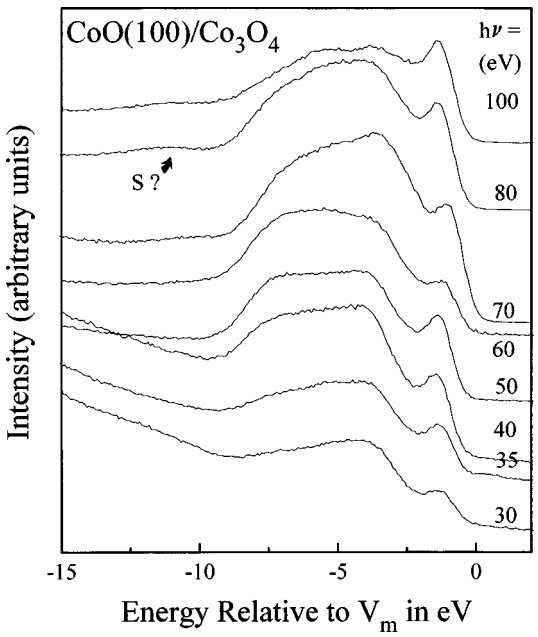

FIG. 6. Photoemission from the Co_3O_4 epitaxy taken at normal emission and as a function of primary beam energy. The feature indicated by *S*? is potentially associated with $3d^{n-1}$ final state.

V. REVERSIBILITY OF THE CoO/Co_3O_4 SURFACE OXIDATION

If Co_3O_4 can be formed by slowly annealing CoO(100) under oxygen, it might be expected that subjecting the $CoO(100)/Co_3O_4$ epitaxy to reducing conditions might regenerate the original CoO(100) surface. This is partially true, as can be seen from the photoemission data in Fig. 7, for which the $CoO(100)/Co_3O_4$ epitaxy is annealed to increasing temperatures under UHV until steady state is achieved. Reduction in UHV initially results in a broadening and decrease in intensity of the $3d^n\underline{L}$ state at the valence-band edge, the maximum of which eventually shifts to -1.7 eV as observed for CoO(100). After the surface has been annealed at 973 K, the general features of the spectrum are similar to those of the CoO(100) substrate, although the background slopes very

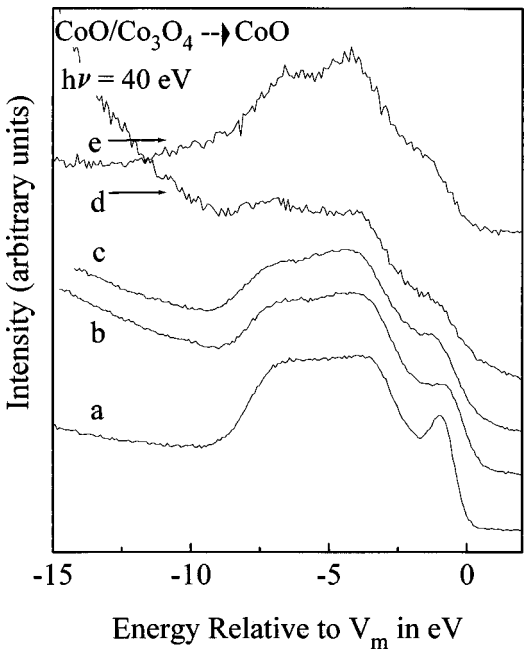

FIG. 7. Photoemission from the valence-band region of the $CoO(100)/Co_3O_4$ surface as it is heated to progressively higher temperatures: (a) no heating, (b) 773 K, (c) 873 K, (d) 973 K and (e) 1073 K. Spectra were acquired at normal emission and 40 eV primary photon beam.

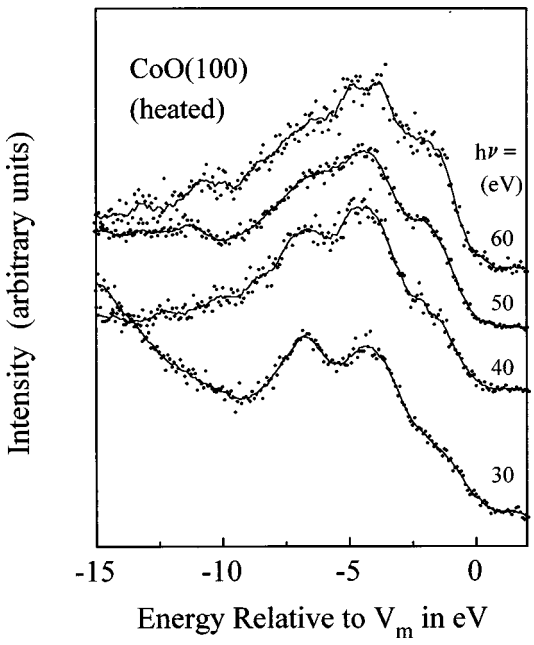

FIG. 8. Photoemission from the CoO(100) surface regenerated from the Co_3O_4 epitaxy by heating to 1070 K. The solid line is a five-point Savitzky-Golay smoothing of the data.

severely, perhaps obscuring the $3d^6$ satellite found for the monoxide at -10.4 eV. The sloping background and overall noisy quality of the spectrum accompany problems in surface charging, a general characteristic of the CoO(100) substrate.

Continued annealing at higher substrate temperatures ameliorates charging problems somewhat, as can be seen in Fig. 7(e) taken after annealing under UHV at 1123 K. As the background intensity becomes more manageable, the -10.4 eV satellite of the cobalt monoxide substrate becomes evident, although it is not as intense as that obtained prior to the oxidation/reduction cycle (Fig. 1). However, photoemission data can still only be obtained at the lower range of photon excitation energies used in the present studies (Fig. 8). The -5.1-eV O $2p$-derived peak also appears more intense in this spectrum, although a large part of this is due to the less strongly sloped background which adds disproportionately to higher binding energies in the spectrum. The remaining peak shapes and energies are comparable to that observed for CoO(100).

VI. DISCUSSION

Few studies elucidating the valence band structure of spinel materials have been reported in part due to the difficulty of modeling unfilled, strongly electron correlated *d*-band materials with unit cells of 56 atoms but also due to difficulties in obtaining appropriate single crystal substrates. Despite the ease with which CoO can be oxidized to Co_3O_4 and its greater importance in many heterogeneous processes, such as partial oxidation catalysis, no careful photoemission studies have been performed on well-ordered Co_3O_4 substrates. The $CoO(100)/Co_3O_4$ epitaxies reported in this study yield Auger and XPS O/Co intensity ratios indicating they are stoichiometrically equivalent to Co_3O_4. Previous HREELS analysis[23] showed a Fuchs-Kliewer phonon structure of similarly prepared oxide thin films that agrees with long-range ordered Co_3O_4 formation. XPS of the core-level Co $2p$ (Fig. 4) is also characteristic of Co_3O_4, including satellite structure on the Co $2p$ peaks. LEED, detected visually here, shows that the epitaxy retains cubic order, although charging problems and non-optimum experimental set-up on the synchrotron end station preclude detailed analysis of complex fine structure resulting from the large spinel unit cell.

Changes in CoO(100) photoemission upon oxidation correlate well with the formation of the spinel Co_3O_4 and the valence-band structure can be rationalized by simple application of ligand field theory. Angle-integrated UPS studies of heavily-oxidized cobalt foil show comparable band structure at the valence band edge and the authors of the study[21] gave the final state assignments reported here along the bottom of Fig. 5. Photoemission studies of polycrystalline $LiCoO_2$,[20] which contains Co^{3+} low-spin $3d^6$ cations in near-octahedral symmetry, also show similar spectra to those reported here for Co_3O_4. These similarities include a shift to lower energy for the valence band maximum peak compared to that observed on CoO and sharpening of the structure at the valence band maximum observed for the Co_3O_4 epitaxy of the present studies. Thus, while both tetrahedral Co^{2+} and octahedral Co^{3+} $3d$ orbitals might be expected to contribute to the valence band edge of Co_3O_4, the greater contribution appears to be from the octahedral cobalt 3^+ cations.

Antiresonance effects indicate that Co_3O_4 has charge-transfer characteristics in its $3d$ band structure, as do CoO and other rocksalt oxides with octahedrally coordinated metal cations. The -1.0 eV peak at the top of the valence band results from a $3d^6\underline{L}$ final state and although it is not clear from the present set of studies where the $3d^5$ state is to

be found, this structure is also very weak in the core-level Co_3O_4 XP spectrum. The octahedral Co^{3+} of Co_3O_4 are low-spin $3d^6$, a very stable configuration presenting a full t_{2g} sublevel. The final-state configuration of $3d^6\underline{L}$ preserves the full sublevel advantage whereas the $3d^5$ final state does not. CoO, in comparison, has high-spin Co^{2+} with a $(t_{2g})^5(e_g)^2$ initial-state configuration for the $3d^7$ cation, and the $3d^6$ final state can actually lead to a low-spin, filled subshell resulting in a greater intensity for the satellite feature for CoO.

Throughout the oxidation process from CoO to Co_3O_4, the O $2p$-derived band structure remains fairly constant in appearance. This is to be expected since both rocksalt and spinel lattices are fcc close packed in O^{2-} anions. The one obvious difference in their photoemission from the O $2p$ region comes not at either CoO or Co_3O_4 extremes in composition, but at intermediate oxidation times [Fig. 2(b), for example] where a hump-like appearance develops with a spectral intensity maximum of -5.3 eV. While the origin of this spectral feature is unknown, several possibilities can be provided or discounted. The feature is not due to the formation of carbonates or other impurities that would have been detected in XPS and Auger analyses. It is also not likely due to hydroxyls, since these would be observed in HREELS.[22] The feature eventually disappears as surface oxidation saturates, indicating that it is unlikely to be an impurity. Adsorbate species, such as $O^-_{2\,ads}$, O^-_{ads} or other potential intermediates in oxygen gas adsorption which eventually incorporate into the growing lattice, are possible candidate; species similar to $O^-_{2\,ads}$ were previously suggested by HREELS studies.[22] Another possibility is defect-like intermediates in the oxidation process. For example, octahedral Co^{2+} are normal lattice features of CoO but are defects in the spinel, which contains only Co^{3+} in the octahedral sites of the Co_3O_4 lattice. The distribution of occupied tetrahedral Co^{2+} sites and octahedral Co^{3+} sites might not be quite spinel-like at intermediate oxidation times. While the subject of defects at oxide surfaces is definitely interesting, there is presently insufficient information to determine the nature of this intermediate species.

VII. SUMMARY

CoO(100) substrates have been oxidized to Co_3O_4 thin films and the phenomenon followed by studies of the valence-band photoemission structure. The most dramatic changes at the top of the valence band include a sharpening of the peak shape and shift to lower binding energies. The -10.4-eV satellite that has been so well studied in the elucidation of CoO and related oxide band structures also shows a shift to lower binding energies with substrate oxidation with a concurrent decrease in intensity of the peak until it is no longer detectable on the fully oxidized substrate. The fully oxidized surface shows characteristic XPS core photoemission binding energies and satellite structure indicative of Co_3O_4 formation, and the valence band structure of this epitaxial film has been assigned using ligand field theory. The formation of Co_3O_4 is partially reversible and heating under UHV regenerates a defect CoO surface.

ACKNOWLEDGMENTS

We are grateful for support from the National Science Foundation under Contract No. CHE-9616690 and from the University of Nebraska Center for Materials Research and Analysis. Access to the NSLS synchrotron beamline and support in its use were graciously provided by Myron Strongin, Department of Physics, Brookhaven National Laboratory.

*Author to whom correspondence should be addressed. Electronic address: Mlangell@unlinfo.unl.edu

[1] Z.-X. Shen, J. W. Allen, P. A. P. Lindberg, D. S. Dessau, B. O. Wells, A. Borg, W. Ellis, J. S. Kang, S.-J. Oh, I. Lindau, and W. E. Spicer, Phys. Rev. B **42**, 1817 (1990).
[2] S.-P. Jeng, Z. Zhang, and V. E. Henrich, Phys. Rev. B **44**, 3266 (1991).
[3] Z.-X. Shen, C. K. Shih, O. Jepsen, W. E. Spicer, I. Lindau, and J. W. Allen, Phys. Rev. Lett. **64**, 2442 (1990).
[4] A. Fujimori and F. Minami, Phys. Rev. B **30**, 957 (1984).
[5] M. Takahashi and J.-I. Igarashi, Phys. Rev. B **54**, 13 566 (1996).
[6] W. C. Mackrodt, Ber. Bunsenges. Phys. Chem. **101**, 169 (1997).
[7] K. W. Wulser, B. P. Hearty, and M. A. Langell, Phys. Rev. B **46**, 9724 (1992).
[8] J. Hugel and M. Kamal, Solid State Commun. **100**, 457 (1996).
[9] S. Shi and V. Staemmler, Phys. Rev. B **52**, 125 (1995).
[10] H. Zeng, Physica B **212**, 125 (1995).
[11] S. Hufner, P. Steiner, and I Sander, Solid State Commun. **72**, 359 (1989).
[12] J. M. Mckay and V. E. Henrich, Phys. Rev. Lett. **53**, 2343 (1984).
[13] S. Hufner and T. Riesterer, Phys. Rev. B **33**, 7267 (1986).
[14] D. D. Sarma, J. Solid State Chem. **88**, 45 (1990).
[15] R. J. Lad and V. E. Henrich, Phys. Rev. B **38**, 10 860 (1988).
[16] N. B. Brookes, D. S.-L. Law, D. R. Warburton, P. L. Wincott, and G. Thorton, J. Phys.: Condens. Matter **1**, 4267 (1989).
[17] K. Terakura, A. R. Williams, T. Oguchi, and J. Kubler, Phys. Rev. Lett. **52**, 1830 (1984).
[18] G. A. Sawatzky and J. W. Allen, Phys. Rev. Lett. **53**, 2339 (1984).
[19] R. J. Lad and V. E. Henrich, Phys. Rev. B **39**, 13 478 (1989).
[20] J. van Elp, J. L. Wieland, H. Eskes, P. Kuiper, G. A. Sawatzky, F. M. F de Groot, and T. S. Turner, Phys. Rev. B **44**, 6090 (1991).
[21] Y. Jugnet and T. M. Duc, J. Phys. Chem. Solids **40**, 29 (1978).
[22] G. A. Carson, M. H. Nassir, and M. A. Langell, J. Vac. Sci. Technol. A **14**, 1637 (1996); M. A. Langell, C. W. Hutchings, G. A. Carson, and M. H. Nassair, J. Vac. Sci. Technol. A **14**, 1656 (1996).
[23] M. Oku and Y. Sato, Appl. Surf. Sci. **55**, 37 (1992).
[24] M. Lenglet, F. Hochu, and M. H. Tuilier, Solid State Commun. **104**, 793 (1997).
[25] M. Oku, J. Solid State Chem. **23**, 177 (1978).
[26] R. D. Shannon and C. T. Prewitt, Acta Crystallogr., Sect. B: Struct. Crystallogr. Cryst. Chem. **25**, 925 (1969).
[27] G. N. Raiker, C. A. Muryn, and P. J. Hardman, J. Phys.: Condens. Matter **3**, Suppl. A, S357 (1991); E. W. Plummer and W. Eberhardt, Adv. Chem. Phys. **49**, 533 (1982).
[28] See, for example, Figs. 6 and 7 of Ref. 1.
[29] S. J. Oh, J. W. Allen, I. Lindau, and J. C. Mikkelsen, Phys. Rev. B **26**, 4845 (1982).

[30] L. C. Davis, Phys. Rev. B **25**, 2912 (1982).
[31] V. M. Jimenez, A. Fernandez, J. P. Espinos, and A. R. Gonzales-Elipe, J. Electron Spectrosc. Relat. Phenom. **71**, 61 (1995).
[32] C. R. Brundle, T. J. Chuang, and D. W. Rice, Surf. Sci. **59**, 412 (1975).
[33] J. Grimbolt, J. P. Bonnelle, and J. P. Beaufils, J. Electron Spectrosc. Relat. Phenom. **8**, 437 (1976).
[34] Y. Tanabe and S. Sugano, J. Phys. Soc. Jpn. **9**, 766 (1954); P. O'D. Offenhartz, *Atomic and Molecular Orbital Theory* (McGraw-Hill, New York, 1970), p. 244.